AGU PUBLICATIONS

JGR

Journal of Geophysical Research: Space Physics

RESEARCH ARTICLE

10.1002/2014JA020326

Charge balance and ionospheric potential dynamics in time-dependent global electric circuit model

Jaroslav Jánský[1] and Victor P. Pasko[1]

[1]Communications and Space Sciences Laboratory, Department of Electrical Engineering, Pennsylvania State University, University Park, Pennsylvania, USA

Key Points:
- Ionospheric potential and charge dynamics for various charge generators in GEC
- Concept of impulse response of GEC for effective representation of GEC dynamics
- Novel approach to the time-dependent model of GEC in spherical coordinates

Correspondence to:
J. Jánský,
jxj21@psu.edu

Citation:
Jánský, J., and V. P. Pasko (2014), Charge balance and ionospheric potential dynamics in time-dependent global electric circuit model, *J. Geophys. Res. Space Physics*, *119*, doi:10.1002/2014JA020326.

Received 24 JUN 2014
Accepted 20 OCT 2014
Accepted article online 26 OCT 2014

Abstract We have developed a time-dependent model of global electric circuit (GEC) in spherical coordinates. The model solves time-dependent charge continuity equation coupled with Poisson's equation. An implicit time stepping is used to avoid a strict dielectric relaxation time step condition, and boundary conditions for Poisson's equation are implemented to allow accurate description of time evolution of the ionospheric potential. The concept of impulse response of GEC is introduced that allows effective representation of complex time dynamics of various physical quantities in the circuit using model results obtained for instantaneous deposition of a point charge. The more complex problems are then reconstructed using convolution and linearity principles. For a point charge instantaneously deposited at a typical thundercloud altitude the impulse response of the charge density shows induction of the same value and polarity charge at the ionospheric boundary, while charge of the same value but opposite sign is moving down logarithmically with time and neutralizes the source point charge on time scale corresponding to the dielectric relaxation time at altitude of the source point charge. The ionospheric potential is modified immediately with input of the source point charge based on free space solution of Poisson's equation. Then the ionospheric potential relaxes. It is shown that during formation of two main charge centers of the thundercloud, typically represented by a current dipole, the ionospheric potential can be determined from the difference of time integrals of two ionospheric potential impulse responses corresponding to charge locations at the opposite ends of the current dipole. For latitude- and longitude-independent conductivity model, the total charge on the Earth is exactly zero at all times. During cloud-to-ground lightning discharge, the ionospheric potential changes instantaneously by a value proportional to the charge moment change produced by lightning and then relaxes to zero. For a typical charge moment change of 35 C km and lightning frequency 10 s^{-1}, the ionospheric potential changes by 9.3 kV; this value agrees well with the results presented by Rycroft et al. (2007) and Rycroft and Odzimek (2010).

1. Introduction

The global electrical circuit (GEC) is established by the naturally occurring presence of a thin veneer of insulating air (our atmosphere) sandwiched between the highly conducting Earth and the conducting mesosphere/ionosphere [e.g., *Williams*, 2009]. *Wilson* [1921] first suggested that thunderstorms and precipitation from electrified shower clouds are the main generators in the GEC. The GEC is also influenced by upper atmospheric generators, such as the ionospheric dynamo and the high-latitude generator associated with magnetospheric convection [*Roble and Hays*, 1979].

A typical thundercloud with positive charge center positioned above the negative charge center produces upward (toward ionosphere) current flow. The totality of thunderstorms acts together and charges the ionosphere to a potential of several hundred kilovolts with respect to the Earth's surface [e.g., *Dolezalek*, 1972]. This potential difference drives a vertical electric current downward from the ionosphere to the ground in all nonthunderous or fair weather regions, thus closing the global current system in GEC. The fair weather current varies according to the ionospheric potential and the total columnar resistance between the ionosphere and the Earth. *Hays and Roble* [1979] modeled thunderstorms as pairs of positive and negative quasi-static point current sources and quantified the large electric potential difference between ionosphere and the Earth that is maintained by large scale thunderstorms. Recent progress on the global electric circuit is summarized by *Rycroft et al.* [2012] and *Williams and Mareev* [2014].

Modeling of GEC evolved over the last 70 years with some relevant references summarized recently in, e.g., *Mallios and Pasko* [2012]. Analytical thunderstorm model [*Holzer and Saxon*, 1952; *Driscoll et al.*, 1992] was developed for steady state conditions. This model solves the potential distribution in space and time for current dipole source and exponential profile of conductivity. The model gives formula for upward current (conducting current flowing from current dipole upward to ionosphere). The upward current is proportional to the source current and is an exponential function of the ratio of altitudes of dipole sources and characteristic altitude scale of conductivity [*Holzer and Saxon*, 1952; *Driscoll et al.*, 1992]. Mathematical calculations to estimate the current contribution for different types of charge generators existing in the GEC were provided also by *Kasemir* [1994]. The Earth was represented as a sphere with constant potential due to its high conductivity. The calculation of the current budget of the GEC based on this model showed that the generator outputs are balanced by an additional current source which provides the Earth with an equally distributed charge density on its surface and gives it a negative potential value. The results of *Kasemir* [1994] were discussed in comments [*Driscoll and Blakeslee*, 1996; *Williams*, 1996], but despite a numerical error and consecutive overstatements, the basic approach remained correct. *Makino and Ogawa* [1984] developed Earth's GEC model with realistic distribution of thunderstorms and altitude and latitude variations of conductivity. Responses of atmospheric electric field to variations of conductivity profiles were evaluated using this model. Recently, *Kalinin et al.* [2014] analyzed spherical model of the GEC, composed of two conducting spheres representing lower and upper atmospheric boundaries. The well posedness of the model was proven and analytical relation of ionospheric potential as a function of source currents was developed for altitude dependent conductivity.

A time-dependent model that simulates the interaction of a thunderstorm with its electrical environment was introduced by *Browning et al.* [1987]. This model was the first that introduced the spherical geometry with axially symmetric storm. An implicit time stepping was proposed. The analytical techniques were also applied to study the dependence of the solution on the properties of the medium determining two time scales of the problem: one determined by the background electrical conductivity and the other by the time dependence of the source function. In *Stansbery et al.* [1993], similar model was implemented to calculate the electric field and current distribution from a thunderstorm source in the GEC. The model included a hemisphere in which the thunderstorm was located, an atmosphere and ionosphere with anisotropic height-variable conductivities, and a passive magnetic conjugate hemisphere connected with an equalization layer. It is shown that approximately half of the current that reaches the ionosphere flows into the conjugate hemisphere and the rest is redirected to the fair weather portion of the storm hemisphere [*Stansbery et al.*, 1993].

Time-dependent models [*Illingworth*, 1972; *Dejnakarintra and Park*, 1974; *Mareev et al.*, 2008; *Mallios and Pasko*, 2012], operating in cylindrical coordinates locally around thunderstorm, focused on electric field and currents flowing around the thunderstorm during transient lightning discharges. *Dejnakarintra and Park* [1974] evaluated lightning-induced electric fields in the ionosphere using Fourier spectrum of source wave form of electric charges in thunderclouds that are subjected to repeated lightning discharges. *Mareev et al.* [2008] examined the way in which different types of lightning drive current in GEC. *Mallios and Pasko* [2012] calculated charge transfer to the ionosphere and to the ground during thunderstorms accounting for slow accumulation of charge during thunderstorm formation, lightning, and thunderstorm dissipation phases.

An analog quantitative model of the GEC was constructed using PSpice electrical engineering software by *Rycroft et al.* [2007] and *Rycroft and Odzimek* [2010]. Currents (~1kA) above thunderstorms and electrified rain clouds raised the potential of the ionosphere to ~250kV with respect to the Earth's surface. The circuit was completed by currents flowing down through the fair weather region. The effects of lightning and sprites on the ionospheric potential were estimated. It was found that negative cloud-to-ground (CG) discharges increase the ionospheric potential by ~4% and positive CG discharges reduce it by ~3%. The proportionality of ionospheric potential change due to CG lightning discharge as a function of associated charge moment change was demonstrated [*Rycroft and Odzimek*, 2010]. The charge moment change of lightning is the product of the charge transferred and its altitude. The dipole moment of lightning is defined to be twice (i.e., including the image charge in the good conducting ground) the product of the charge transferred to the ground and the altitude from which it was transferred.

The purpose of this paper is to introduce time-dependent spherical model of GEC which allows to self-consistently track the evolution of charge density, electric field, and potential in time. A novel approach

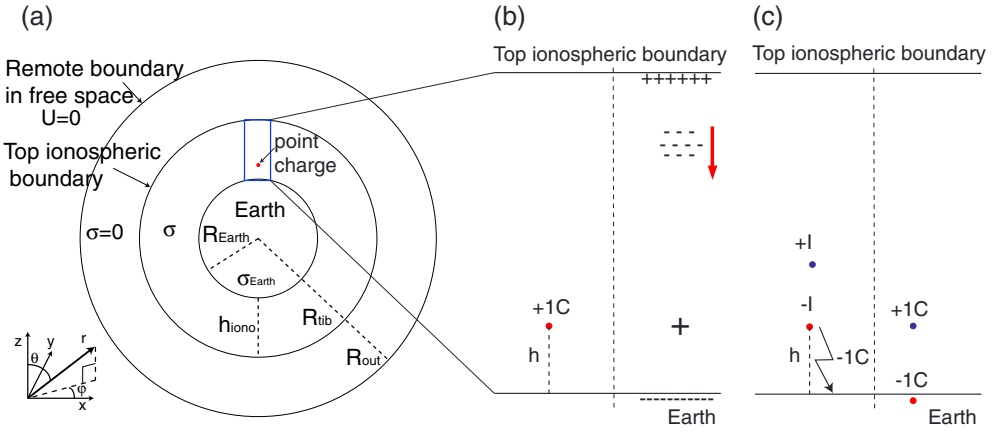

Figure 1. Schematics of the computational domain. (a) Schematically (drawn not to scale) full view of Earth, top ionospheric boundary, and zero potential remote boundary. (b) Zoom in view of the volume close to axis $\theta = 0°$ where the initial point charge is introduced (left) and schematic representation of movement of charges after the source point charge is introduced (right). (c) Zoom in schematics of a thunderstorm as dipole current source (left). When the −CG lightning transfers the negative charge −1 C, a charge dipole is used to represent the −CG lightning discharge as schematically shown in Figure 1c (right).

to boundary conditions is implemented to allow time-dependent development of ionospheric potential from first principles and avoiding approximations typically used in past works on GEC. Additionally, the analysis of a solution for relaxation of an instantaneously deposited point charge is examined from a point of view of impulse response. It is demonstrated that concept of impulse response leads to a significant speedup of simulations with more complex sources when convolution and linearity principles are employed.

In section 2 the model is introduced and described. Section 3.1 shows the impulse response results for instantaneous input of a point charge. In section 3.2 the results representing formation of two main charge centers of thunderstorm using dipole current source are reported, and the same results are then reproduced using the convolution operation utilizing obtained impulse responses. Section 3.3 discusses contribution of a negative cloud-to-ground (CG) lightning to the ionospheric potential. Section 4 provides discussion and interpretation of results.

2. Model Formulation

We introduce a time-dependent axially symmetric spherical model of the electrical behavior of the global electric circuit. The model is based on continuity equation for charge density ρ:

$$\frac{\partial \rho}{\partial t} + \vec{\nabla} \cdot (\sigma \vec{E}) = S_{\text{cur}}\,, \tag{1}$$

and Poisson's equation for the electric potential ϕ:

$$\vec{\nabla}^2 \phi = -\rho/\varepsilon_0\,, \tag{2}$$

where $\vec{E} = -\vec{\nabla}\phi$ is the electric field, σ is the conductivity of the media, S_{cur} is the current source term, and ε_0 is the permittivity of free space. Relative permittivity is constant and equal to 1 everywhere in the simulation domain. The relative permittivity of Earth is assumed to be 1 as a first approximation. We have verified that change of relative permittivity by 1 order of magnitude does not modify the ionospheric potential results presented in this work. The system of equations (1) and (2) is valid assuming that the time derivative of the magnetic vector potential is much less than the gradient of the electric potential [*Jackson*, 1999, pp. 239–246] and is widely used in modeling of GEC [*Browning et al.*, 1987; *Driscoll et al.*, 1992; *Stansbery et al.*, 1993].

The schematics of our simulation domain is shown in Figure 1a. The model employs spherical coordinate system (r, θ, φ) with origin positioned at the center of the Earth at $r = 0$ km. The model domain includes highly conducting Earth, a relatively thin layer (typical model values are $\simeq 100$ km, see below) representing weakly conducting atmosphere and the ionosphere, and a very large free space domain bounded

by a remote spherical shell representing physical condition of zero potential $U=0$ at infinity (Figure 1a). The geometry of the model and implementation of the boundary conditions for Poisson's equation allow to study time evolution of ionospheric potential from the first principles. The ionospheric potential U_{IE} is defined as the difference between average potential on the top ionospheric boundary and average potential on the Earth:

$$U_{IE} = \frac{\oint_{tib} \phi \, dS}{S_{tib}} - \frac{\oint_{Earth} \phi \, dS}{S_{Earth}}, \tag{3}$$

where surface integrals are calculated over the top ionospheric boundary and Earth surfaces, with areas S_{tib} and S_{Earth}, respectively. In the proposed model the only required boundary condition for the Poisson's equation is potential on the outside boundary. We use a zero potential on the outside boundary of the domain which is set very far from the Earth at $R_{out}=1414\,R_{Earth}=9.01\times10^6$ km to approximate zero potential in free space at infinity. Earth is described as a sphere of radius $R_{Earth}=6371$ km in the center of the domain. We implement periodic boundary conditions for φ.

To describe motion of charges inside the system, spatially variable conductivity is introduced. Inside the Earth the conductivity is set to $\sigma_{Earth} = 10^{-6}\,S\,m^{-1}$. This conductivity is artificially chosen as first approximation to be sufficiently high to allow evolution of charge inside the Earth on timescales faster than the times of ionospheric potential variation. In the air above the Earth surface the exponential approximation of the conductivity is used [*Dejnakarintra and Park*, 1974]:

$$\sigma(h) = 5\times10^{-14}\,e^{h/l}\,S\,m^{-1}, \tag{4}$$

where h is the altitude and $l=6$ km is the altitude scaling distance. Then $R_{tib}=R_{Earth}+h_{iono}$, where $h_{iono}=100$ km describes radial distance corresponding to the top of the model ionosphere. Above R_{tib}, in the area considered as free space, the conductivity is set to zero. Zero conductivity of free space surrounding GEC keeps charge confined to GEC. The specific choice of h_{iono} and R_{tib} values does not affect any results presented in the present work. *Tzur and Roble* [1985] indicated the importance of the equalization layer in spreading the current output from the thunderstorm and in maintaining global fair weather conditions. The altitude 100 km of top ionospheric boundary is chosen to correspond to sufficiently high conductivity so that the whole top ionospheric boundary will behave with good accuracy as an equipotential layer. We emphasize the importance of accurate model representation of the highly conducting ionosphere for correct description of charge flow and redistribution in this system. In reality, various processes contribute to charge redistribution in ionosphere [*Tzur and Roble*, 1985; *Stansbery et al.*, 1993]. Our high-altitude boundary captures principal dynamics of the real system by employing exponential conductivity profile and simple boundary conditions.

The domain is split in spherical structured mesh characterized by cell centers $(r,\ \theta,\ \varphi)$. In radial direction inside the Earth the mesh step is 100 km. Close to the Earth surface the step is decreased exponentially with factor 1.15 to the size 100 m on the Earth surface. Above the Earth surface the homogeneous mesh step of 1 km is used until the top ionospheric boundary is reached and then mesh step exponentially expands with a factor of 1.1 until the end of the domain at R_{out}. In the direction of latitude, the θ mesh near $\theta=0°$ has a constant step of 0.0045° corresponding to 0.5 km mesh size on Earth surface. The model sources are input at $\theta=0°$, and we take advantage of axial symmetry. Then from $\theta=0.27°$ the mesh is exponentially expanded with a factor 1.1 until it reaches step 1.8° corresponding to step 200 km on the Earth surface which is then kept constant. Under these symmetric conditions, only one cell $(0,\ 2\pi)$ is required to describe the direction in longitude φ. The overall number of $(r,\ \theta,\ \varphi)$ grid points used in the present study is $(325,\ 211,\ 1)$.

The equations (1) and (2) are discretized in space using finite volume method [*LeVeque*, 2002]. This method is conservative and is chosen to ensure precise charge conservation. The scalar variables (charge density and potential) are defined at cell centers, while vector variables (electric field and current density) are defined on cell interfaces (more accurately at centers of those interfaces). The simulation inputs are defined as used by equations, the current source term S_{cur} is defined in cell centers, and conductivity on cell interfaces. The gradient of potential and electric field E_j in the direction of increasing index j are discretized as

$$\vec{\nabla}\phi_{j,j+1} = -\vec{E}_j = \frac{\phi_{j+1}-\phi_j}{\Delta}\vec{a}_j, \tag{5}$$

where ϕ_j corresponds to the potential at the center of jth cell, $\vec{a}_j$ is a unit vector of direction of index j and Δ corresponds to the distance between centers of j and $j+1$ cell.

For time discretization the implicit method is used [*Browning et al.*, 1987; *Stansbery et al.*, 1993]. This method of time advancement is free of time step constraints and allows significant freedom in choosing time step depending on the physical regime of interest. For advancement from t^n to t^{n+1} with the time step Δt, first, the charge density in every cell is updated due to the source current term:

$$\rho^{n+1,*} = \rho^n + \Delta t\, S_{cur}\,. \tag{6}$$

Then the charge density has to be advanced in time due to current density $\vec{J} = -\sigma\,\vec{\nabla}\phi$:

$$\rho^{n+1} = \rho^{n+1,*} + \frac{\Delta t}{V}\oint_S \sigma\vec{\nabla}\phi^{n+1}\cdot \mathrm{d}\vec{S}, \tag{7}$$

where V is the volume of each cell and S is the surface of each cell. It is important to note that ϕ^{n+1} is taken implicitly at a new time t^{n+1} and is not known yet. The Poisson's equation (2) in integral form (i.e., Gauss's law) at time t^{n+1} is as follows:

$$\oint_S \varepsilon_0\vec{\nabla}\phi^{n+1}\cdot \mathrm{d}\vec{S} = -\rho^{n+1}\,V. \tag{8}$$

Substituting ρ^{n+1} from equation (7) to equation (8) results then in an equation with one unknown ϕ^{n+1}:

$$\oint_S \left[(\varepsilon_0 + \Delta t\,\sigma)\vec{\nabla}\phi^{n+1}\right]\cdot \mathrm{d}\vec{S} = -\rho^{n+1,*}\,V. \tag{9}$$

Having solved equation (9) for ϕ^{n+1}, a new charge density ρ^{n+1} is evaluated from equation (7). The equations have to be solved for each cell in the domain. Surface integrals are replaced with sums over the faces of the cells. Equations (6) and (7) are solved for each cell independently. The equation (9) features spatial gradient of unknown potential ϕ^{n+1} which means that equation for every cell includes also the neighbor's cell unknown and it results in a large sparse linear system of equations and is solved using direct solver MUMPS [*Amestoy et al.*, 2001]. For simulations targeting description over all possible timescales, we use exponential advancement in time (in units of seconds):

$$t^n = 10^{-7+0.01*n}\,. \tag{10}$$

We have compared the results of ionospheric potential for this time advancement with 10 times finer one, and the error was less than 0.1%. For calculations involving operation of convolution (see below), a constant time step $\Delta t = 10^{-3}$ s is used, also leading to error less than 0.1%.

The system of equations (1) and (2) forms an initial boundary value problem and is linear as conductivity σ is not a function of any unknowns (ρ, ϕ, $\vec{E}$). The evolution of a linear system after short input signal is called impulse response in signal processing [*Lyons*, 1997, p. 165]. In the context of GEC, we simulate impulse response of the system after instantaneous input of source point charge at $t = 0$. In our simulations the source point charge is placed on axis $\theta = 0$ to take advantage of symmetry, but the concept is valid for any placement. We assume the source currents on the right-hand side of equation (1) equal to zero to study only the response to the input charge. We refer to the evolution of such system as impulse response to the instantaneous input of charge.

Analogically, from the mathematical point of view, the instantaneous input of source point charge is represented by the delta functions in time and space and can be written as $S_{cur} = Q\,\delta(\vec{r} - \vec{r}_0)\,\delta(t)$, where Q is the charge and $\vec{r}_0$ corresponds to the position vector where the point charge is inserted. Then the equation (1) with delta function right-hand side S_{cur} is in a form of inhomogeneous linear differential equation used for definition of Green's function [*Arfken and Weber*, 2012, p. 447]. The impulse response solution is therefore equivalent to the Green's function. In this paper we use impulse response terminology and emphasize direct analogy of our solutions with Green's function formulation. In the past, the spatial Green's function was considered in quasi-static GEC model calculations [*Hays and Roble*, 1979].

We assumed zero source currents in the discussion in the previous paragraph to introduce the concept of impulse response. To obtain the behavior of complex systems including source currents, we consider

point source currents at position $\vec{r}_0$ as a sequence in time of instantaneous inputs of point source charges at the same location. Then the problem can be solved using convolution operation of precalculated impulse responses corresponding to spatial location of source current and source currents themselves. For example, the solution of potential $\phi(\vec{r}, t)$ at arbitrary position $\vec{r}$ and at time t is then the convolution ($*$) of potential impulse response $\phi^{\mathrm{IR}}(\vec{r}, t)$ and source current $I(t)$ on time interval $(0,\ t)$:

$$\phi(\vec{r}, t) = I(t) * \phi^{\mathrm{IR}}(\vec{r}, t) = \int_0^t I(\tau)\, \phi^{\mathrm{IR}}(\vec{r}, t-\tau)\, \mathrm{d}\tau\,. \tag{11}$$

The impulse response ϕ^{IR} corresponds to the instantaneous input of source point charge of 1 C at the same spatial position as the location of the point source current $I(t)$. The impulse response in this case is equal to potential per unit charge and has the dimension V C^{-1}. The point source current $I(t)$ is connected to the current source term as $S_{\mathrm{cur}} = I(t)\, \delta(\vec{r} - \vec{r}_0)$. Same procedure is valid for other unknowns, electric field $\vec{E}$ and charge density ρ.

In this work, sources are assumed to be point charges or point currents. The solutions for more complex spatial distributions of sources can be reconstructed using linearity principles as linear combination (or integral for continuous source function) of solutions corresponding to point charges. For example, the ionospheric potential $U_{\mathrm{IE}}(t)$ caused by N source currents I_j at N different positions h_j is written as follows:

$$U_{\mathrm{IE}}(t) = \sum_{1 \le j \le N} I_j(t, h_j) * U_{\mathrm{IE}}^{\mathrm{IR}}(t, h_j)\,, \tag{12}$$

where $U_{\mathrm{IE}}^{\mathrm{IR}}(t, h_j)$ is the impulse response of ionospheric potential to the instantaneous input of source point charge of 1 C at position h_j.

In this work we first present calculations of the impulse response to the simplest element, namely, instantaneous input of source point charge of 1 C. Following that we show how convolutions and linear combinations of impulse responses allow to efficiently construct the solutions of more complex problems in GEC including formation of two main charge centers of the thunderstorm and negative cloud-to-ground lightning discharge. The presented new formulation provides a straightforward physical interpretation of these problems.

3. Results

3.1. Impulse Response of a Point Charge

In this section the impulse response of the GEC to the instantaneous input of a point charge at $t = 0$ s is described. Impulse response of a physical quantity of interest is calculated per unit input charge 1 C allowing easy scaling of results for any charge of interest. As illustrated in Figures 1a and 1b, the point charge of 1 C is introduced inside the cell with the center at altitude $h = 9.5$ km. First cell next to the axis $\theta = 0°$ (cell center is at $r = 6380.5$ km and $\theta = 0.0022°$) is used to take advantage of the axial symmetry. The source charge density inside this cell is 1 C divided by the volume of the cell: 1.27×10^{-9} C/m^3.

The charge density shows multiscale behavior in time and space. Therefore, the exponentially increasing time instants are chosen and spatial plots are separated to show the view of full Earth and zoom in view around the source point charge for better representation. In Figure 2 the two-dimensional view of charge density is shown for four different instants of time 10^{-4}, 10^{-2}, 10^{0}, and 10^{2} s. The right-hand side of each panel ($x > 0$ km) corresponds to $\varphi = 0°$, and the left-hand side ($x < 0$ km) to $\varphi = 180°$ (due to symmetry of the problem, the results are symmetric). In Figures 2e–2h a view of the full Earth is shown. The radial coordinate is transformed as $r^* = r - R_{\mathrm{Earth}} + 100$ km for better visual representation.

The behavior of charge density in the proximity of the source point charge is illustrated in Figures 2a–2d. First at $t = 10^{-4}$ s the positive charge is induced on the top ionospheric boundary and negative charge is induced immediately under the top ionospheric boundary. Then, as the time increases to $t = 10^{-2}$ s, negative charge is moving down to lower altitudes with lower conductivity. The positive charge density at the top ionospheric boundary is reduced but is still positive. At $t = 10^{0}$ s, the positive and negative charges are located mostly around the source point charge and the neutralization of source point charge begins. At $t = 10^{2}$ s the charge density at source point charge location is reduced to values under 10^{-10} C/m^3. At $t = 10^{4}$ s (not shown on figures) the charge density is negligible around the location of source point charge.

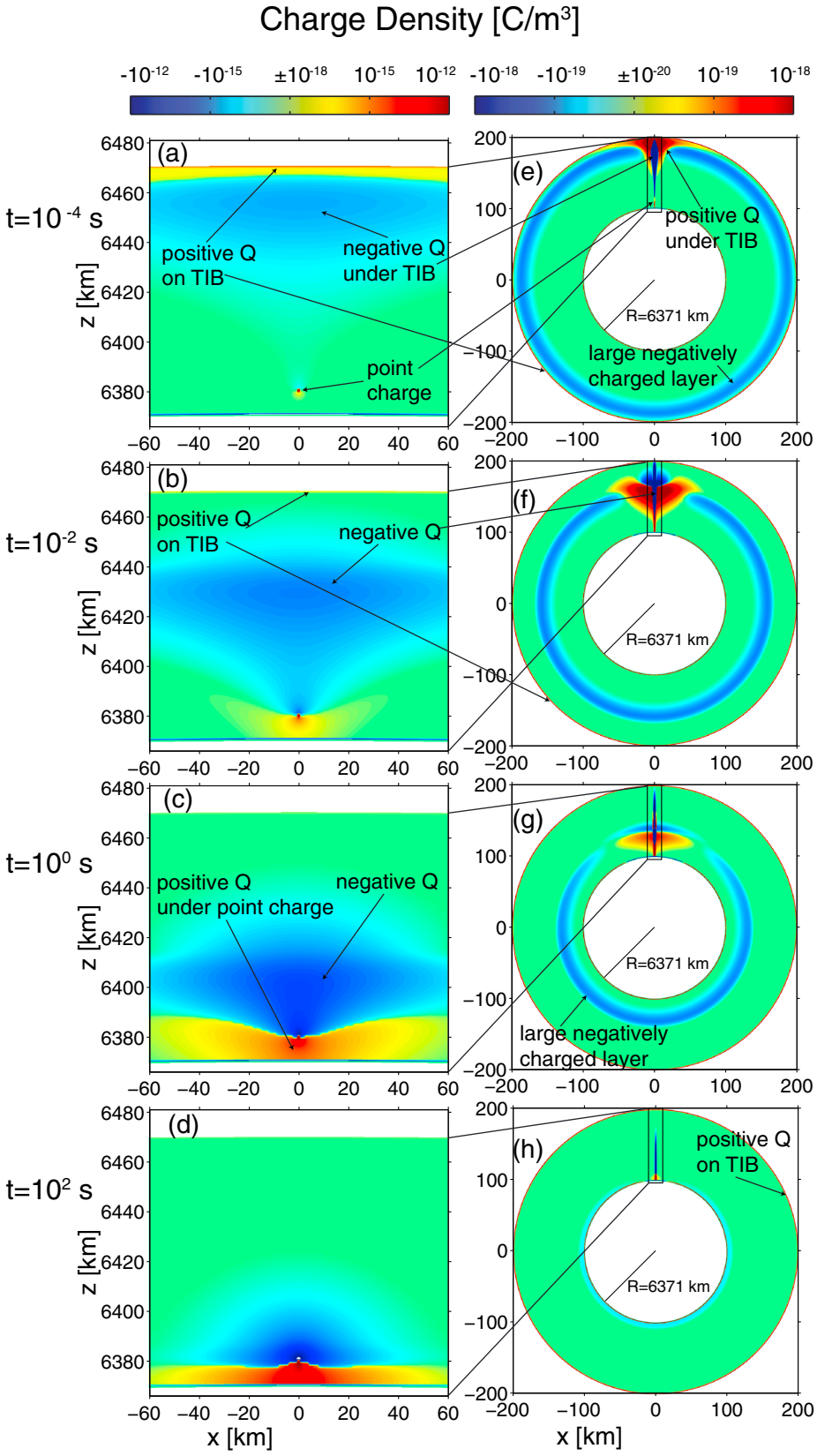

Figure 2. Two-dimensional view of charge density. Zoom in view of volume around source point charge at times (a) 10^{-4}, (*b*)10^{-2}, (*c*)10^{0} and (d) 10^{2} s. (e)–(h) View of full Earth at corresponding times. For convenience of presentation the radial coordinates are transformed as $r^* = r - R_{\mathrm{Earth}} + 100$ km.

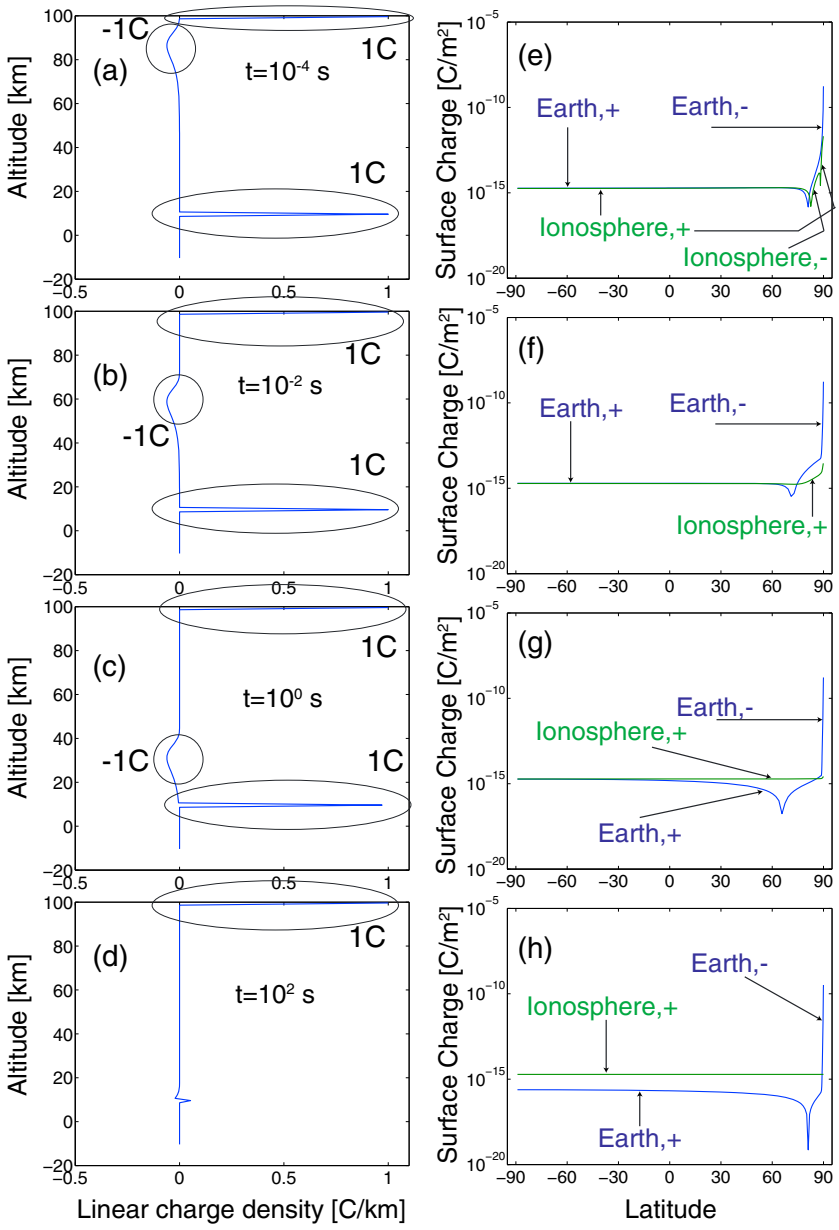

Figure 3. (a)–(d) Horizontally integrated (over θ and φ) linear charge density as a function of altitude, which correspond to times 10^{-4}, 10^{-2}, 10^{0}, and 10^{2} s. The total charges over circled altitude intervals are evaluated and labeled. (e)–(h) Surface charge density ρ_S on the top ionospheric boundary (Ionosphere, $\rho_{S,TIB}$) and Earth surface (Earth, $\rho_{S,Earth}$) at respective times as a function of latitude. The source point charge is located at latitude 90° corresponding to $\theta = 0°$. The magnitude of surface charge density is plotted using logarithmic scale and the sign of charge is marked explicitly by a plus or minus sign.

Observed behavior of negative charge movement to lower altitudes with lower conductivity can be understood using a moving capacitor plate model presented by *Greifinger and Greifinger* [1976]. The time at which the negative charge is present at given altitude corresponds to the dielectric relaxation time at that altitude. It means that for exponential conductivity profile, defined by equation (4), linear decrease of negative charge altitude h_- with logarithmic increase of the time t ($t < \varepsilon_0/\sigma_0$) is expressed as follows [*Hale and Baginski*, 1987; *Pasko et al.*, 1997, equation (B6)]:

$$h_-(t) \simeq -l \ln\left(\frac{\sigma_0 t}{\varepsilon_0}\right), \tag{13}$$

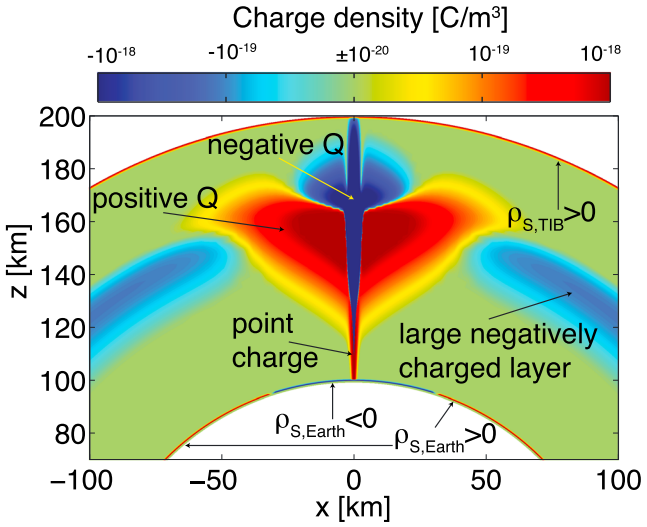

Figure 4. Two-dimensional view of charge density at time 10^{-2} s. For convenience of presentation the radial coordinates are transformed as $r^* = r - R_{\text{Earth}} + 100$ km. Surface charge density on the top ionospheric boundary is labeled $\rho_{\text{S,TIB}}$ and on Earth surface is $\rho_{\text{S,Earth}}$.

where σ_0 refers to conductivity on Earth surface 5×10^{-14} S m^{-1} and l is the altitude scaling distance defined after equation (4). The moving charge layers above lightning producing thundercloud are observed and described also in [*Riousset et al.*, 2010].

In Figures 2e–2h the impulse response of charge density around full Earth is illustrated. It is important to note that the rectangles drawn around the source point charge schematically representing the area of zoom in view of Figures 2a–2d, do not correspond to the actual limits of zoom in views. In Figures 3e–3h the surface charge density distribution along the top ionospheric boundary and Earth surface is illustrated to complement two-dimensional plots. Apart from the area located in proximity of the source point charge, the behavior of charge density is essentially one-dimensional in r as it varies only in vertical direction. The one-dimensional behavior of the charge density is represented by a large negatively charged layer in the atmosphere around most of the Earth. In Figure 2e at $t = 10^{-4}$ s, the complex structure of charge is induced on the top ionospheric boundary and under it. Three regions are identified. First, above the source point charge for $\theta \leq 10^{-1\circ}$, the positive charge is induced on the top ionospheric boundary and the negative charge is induced under it as presented in Figure 2a. For $\theta \sim 1°$ the negative charge is induced on the top ionospheric boundary and the positive charge is induced under. For $\theta > 10°$, one-dimensional area, positive charge is induced on the top ionospheric boundary and the large negatively charged layer is induced under. The surface charge on Earth is composed of high negative surface charge located just under the source point charge. The surface charge then drops by 5 orders of magnitude outside of the immediate vicinity of the source, and a small positive surface charge is observed in the rest and most of the domain. It is interesting to note that surface charge densities on Earth surface and top ionospheric boundary have the same positive sign and are equal in fair weather region. At $t = 10^{-2}$ s all volume charges are moving in the direction toward lower altitudes, and the top ionospheric boundary is positively charged everywhere. In Figure 4 charge density at $t = 10^{-2}$ s is illustrated in midrange view for better visual representation of all spatial scales together. With the time increasing it is observed in Figures 2e–2h, how the large negatively charged layer is moving down analogically to a moving capacitor plate model presented by *Greifinger and Greifinger* [1976]. It is interesting to note that for $t = 10^2$ s the large negatively charged layer reaches the Earth, neutralizes the surface charge on Earth's surface, and the only significant volume charge is now located around the source point charge. At $t = 10^4$ s (not shown on Figure 2) all the volume charge disappears and the system reaches a convergent state with all charge located on the top ionospheric boundary.

To better understand the behavior of the charge, in the Figures 3a–3d, the horizontally integrated (in θ and φ over whole Earth) linear charge density as a function of altitude is shown. The linear charge density shows three distinct altitude areas and is integrated over them, to obtain total charge in each of them, as marked by circled areas in the Figures 3a–3d. At $t = 10^{-4}$ s it is seen that at $h = 9.5$ km the charge is equal to source point charge 1 C. At the top ionospheric boundary the charge of the same sign and value 1 C is induced. Under the top ionospheric boundary the negative charge is spread over several kilometers of altitude, but in total it gives charge −1 C to conserve the total charge in the domain. This negative charge is formed dominantly from the large negatively charged layer, while the charges close to the source point charge contribute less. The negative charge is moving down with increasing time. At $t = 10^0$ s the negative charge is reaching the position of the source point charge, and at $t = 10^2$ s the source point charge is almost neutralized.

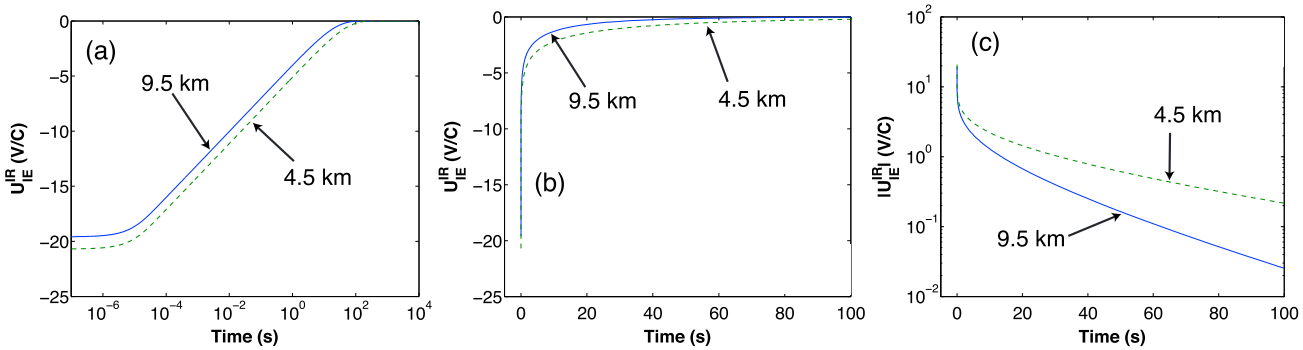

Figure 5. Impulse response of ionospheric potential U^{IR}_{IE} corresponding to deposition of a source point charge 1 C located at altitude $h = 9.5$ km (full line) and 4.5 km (dashed line). Different formatting used to effectively represent different scales of physical system: (a) logarithmic t—linear U^{IR}_{IE}, (b) linear t—linear U^{IR}_{IE}, and (c) linear t—logarithmic $|U^{IR}_{IE}|$.

This is not in contradiction with results on Figure 2d where the charge around the source is still present, but it is small compared to the total charge 1 C. All the charge 1 C is then located only on the top ionospheric boundary. It is interesting to note also that spatial distribution of surface charge on Earth at all times (see Figures 3e–3h) is variable, but the total surface charge on Earth is zero at all times (see Figures 3a–3d for altitude 0 km).

The ionospheric potential is defined by equation (3) as the difference between average potentials on the top ionospheric boundary and on Earth. The time evolution of ionospheric potential related to the case of point charge 1 C instantaneously deposited at altitude $h = 9.5$ km is shown in Figures 5a–5c with solid line. It is seen in Figure 5a that the ionospheric potential remains constant for $t < 10^{-5}$ s. This value corresponds to the difference between average potential on the Earth and average potential on the top ionospheric boundary, where the potential of point charge is simply solved in free space (no other charge is yet induced in the system), schematically represented in Figure 1a. The ionospheric potential is negative, which means that the average potential on the Earth is higher than the average potential on the top ionospheric boundary. This is valid for every position of point charge in between the Earth and the top ionospheric boundary, and the explanation is presented in Appendix A. It is important to note that surface charge on Earth is induced very fast but as the total surface charge of Earth is zero (see Figures 3a–3d for altitude 0 km), the ionospheric potential is not modified. Then as the time reaches the dielectric relaxation time scale of the top ionospheric boundary 10^{-5} s, the charge in and under the top ionospheric boundary starts to be induced and modifies the ionospheric potential. It is seen that the absolute value of ionospheric potential is decreasing linearly with logarithm of time (for $t < 10^{0}$ s) analogically to the altitude of negative charge −1 C as seen in Figures 3a–3c. The relation of the charge altitude and ionospheric potential is demonstrated later in this section. Then from Figure 5c it is seen that the absolute value of the ionospheric potential drops approximately exponentially for times $t > 10$ s. The decrease is not exactly exponential, and the characteristic times are in the range of 20% from the dielectric relaxation time corresponding to the altitude of the source point charge—$t_{DRT} = 36.3$ s at $h = 9.5$ km. At the convergent state, all the charge is homogeneously distributed over the top ionospheric boundary and the system behaves as a spherical conductor. The potential of the spherical conductor charged with 1 C with the radius of the top ionospheric boundary $R_{Earth} + h_{iono}$ is then as follows:

$$\frac{1}{4\pi\varepsilon_0}\frac{1\,\mathrm{C}}{(R_{\mathrm{Earth}} + h_{\mathrm{iono}})} = 1.39\,\mathrm{kV}\,. \tag{14}$$

As the potential inside the conducting sphere is constant, the potential on the top ionospheric boundary is equal to the potential on the Earth surface and the ionospheric potential is equal to zero.

In Figures 5a–5c, impulse response of ionospheric potential corresponding to sudden introduction of source point charge at altitude 4.5 km is also illustrated. It is seen that impulse response corresponding to the lower altitude source point charge has higher negative peak value (corresponds to free space solution) and is relaxing longer. The peak values obtained from simulation are shown in Figure 6a. It is seen that peak values

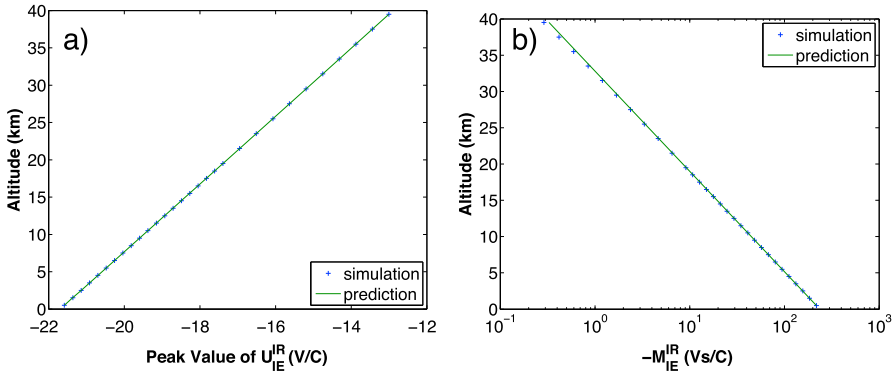

Figure 6. (a) Peak value of ionospheric potential impulse response (corresponding to free space solution) as a function of altitude of the source point charge. The prediction function is almost linear and plotted from equation (15). (b) M_{IE}^{IR}—time integral of ionospheric potential impulse response U_{IE}^{IR} as a function of altitude of the source point charge. The prediction function is decreasing exponentially and plotted from equation (16).

almost follow linear dependence on height. However, a small correction in the denominator of prediction function has to be introduced to reproduce simulation data:

$$U_{IE}^{IR}(h) = \frac{h - h_{iono}}{4\,\pi\,\varepsilon_0\,\left[R_{Earth}^2 + R_{Earth}(h_{iono} + h) + h_{iono}\,h\right]}\,. \tag{15}$$

This analytical prediction is described and proved in Appendix A in the form of equation (A2). Linear decrease of the absolute value of the ionospheric potential with logarithm of time in Figure 5a then corresponds to a linear decrease of negative charge altitude with logarithm of time as seen in Figures 3a–3d.

As will be demonstrated later in sections 3.2 and 3.3, M_{IE}^{IR}, the time integral (from $t = 0$ to ∞) of ionospheric potential impulse response is a very important quantity. In Figure 6b, altitude dependence of this time integral is shown. This integral can be directly interpreted in terms of area enclosed above the curves and below the top horizontal axis in the linear plots of Figure 5b. It is found that the short time scales do not contribute to the integral, and it is mostly the exponential drop phase which contributes to the integral value. During the exponential drop phase the absolute value of the ionospheric potential drops exponentially with characteristic time similar to the dielectric relaxation time at the altitude of the source point charge

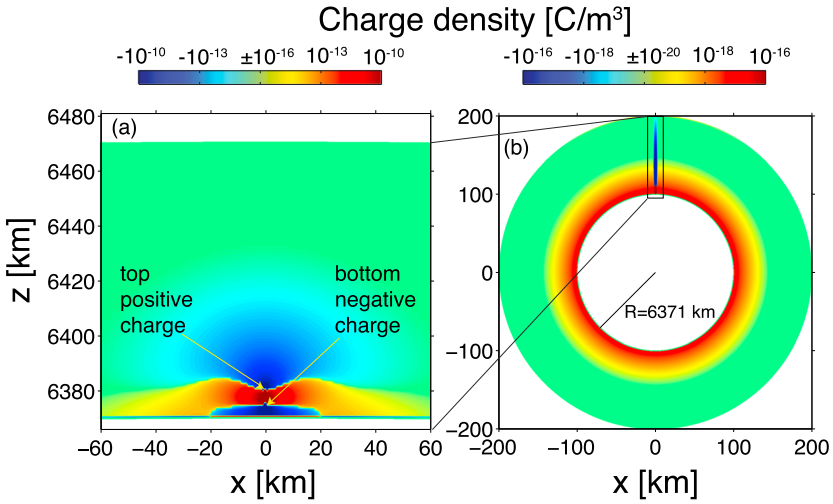

Figure 7. Two-dimensional view of charge density at steady state of thunderstorm charging phase. (a) Zoom in view of volume around source current dipole. (b) View of full Earth. The radial coordinates of full view are transformed as $r^* = r - R_{Earth} + 100\,\text{km}$.

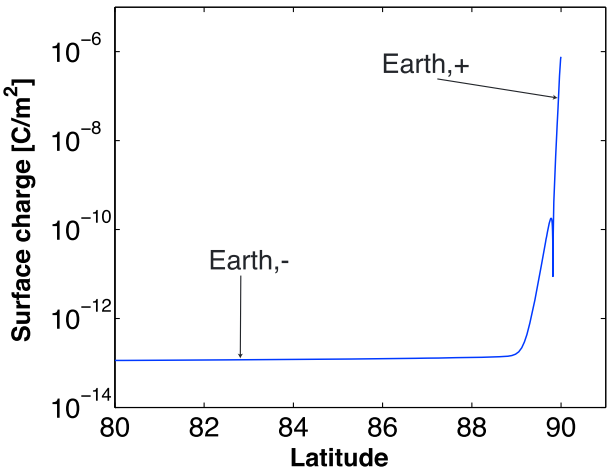

Figure 8. Surface charge density distribution on Earth surface as a function of latitude for the case of steady state current dipole source depicted in Figure 1c. The surface charge density is plotted on logarithmic scale and sign of charge is explicitly marked by a plus or minus sign.

(see discussion related to Figure 5c). Then the prediction function can be formed to characterize the exponential dependence:

$$M^{\mathrm{IR}}_{\mathrm{IE,prediction}}(h) = \frac{M^{\mathrm{IR}}_{\mathrm{IE}}(h_{\mathrm{ref}})}{\exp\left(\Delta h/l\right)}, \qquad (16)$$

where $\Delta h = h - h_{\mathrm{ref}}$ is the altitude difference from the reference point and $l = 6$ km is the scaling distance of conductivity. The altitude of the reference point can be chosen arbitrarily, but lower altitudes are preferred as the prediction function gives better fit for lower altitudes than for higher altitudes. For the prediction function plotted in Figure 6b, the lowest altitude point is chosen as $h_{\mathrm{ref}} = 0.5$ km. It is seen that for low altitudes the prediction function is very well correlated with simulation data and therefore confirms exponential dependence of time integral of ionospheric potential impulse response with altitude of source point charge. For higher altitudes with more than 2 orders of magnitude smaller integrals, small differences appear. For higher altitudes the exponential drop phase is faster and then contribution of initial logarithmic part of impulse response is relatively higher and violates the assumptions for equation (16). For example, the integral calculated from simulation at $h = 39.5$ km deviates by 10% from the predicted data.

3.2. Formation of Two Main Charge Centers of the Thunderstorm

In this section the formation of two main charge centers of the thunderstorm, also referred to as charging phase, is studied. The processes leading to charge separation inside the cloud are represented by a source current dipole [*Holzer and Saxon*, 1952; *Tzur and Roble*, 1985]. The schematics is shown on Figure 1c. The source current dipole is placed at $\theta = 0°$. Positive current $I_s = 1$ A is placed in a cell with center at altitude $h = 9.5$ km, and negative current $-I_s = -1$ A is placed in a cell with center at altitude $h = 4.5$ km. Mathematically these initial conditions evolve to a steady state solution with one current dipole source supporting the global electric circuit. This case is chosen to demonstrate the use of convolution to represent steady state using available impulse responses and to show the relation of ionospheric potential impulse response on ionospheric potential during thunderstorm charging phase. We note that in the present model case, both currents are turned on at $t = 0$ and stay constant. The presented formulation allows straightforward generalization for currents with arbitrary time variation.

In Figure 7a charge density spatial distribution around the source current dipole is illustrated during steady state of thunderstorm charging phase. Steady state is obtained from time-dependent model at sufficiently long time $t = 10^4$ s. The distribution is composed mostly of bottom negative charge and top positive charge self-consistently produced at positions of negative and positive current sources, respectively. This distribution is consistent with previously reported results for single thunderstorm [e.g., *Hays and Roble*, 1979] and agrees well with profiles of charge density presented by *Rycroft and Odzimek* [2010, Figure 13b]. Negative charge density is observed under and above, while positive charge density is observed in between current sources. It is important to note that in steady state the total charge around the current source dipole is negative due to dominance of bottom negative charge (see additional discussion on dependence of charge density on ambient conductivity in *Holzer and Saxon* [1952, equation (8)] or *Riousset et al.* [2010]).

In Figure 7b, charge density spatial distribution over full Earth is illustrated during steady state of thunderstorm charging phase. It is observed that most of the charge in fair weather region is positive and resides close to the Earth surface as observed in, e.g., *Rycroft and Odzimek* [2010]. In Figure 8 the surface charge density on Earth surface corresponding to the steady state is shown. The charge on Earth surface just under the dipole at $\theta = 0°$ (latitude 90°) is high and positive. The charge on the rest of the Earth is smaller, almost constant and negative. In total the surface charge on Earth Q_{Earth} is equal to zero. This can be understood by

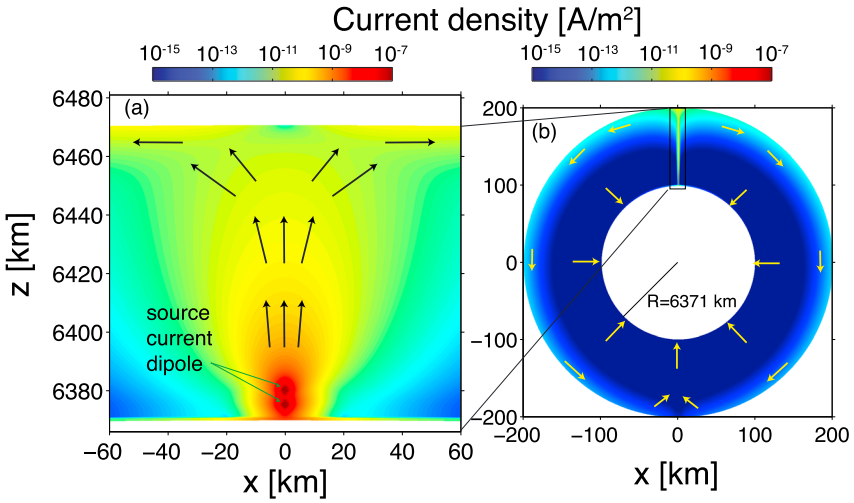

Figure 9. Two-dimensional view of current density at steady state of thunderstorm charging phase. (a) Zoom in view of volume around the source current dipole. (b) View of full Earth. The black (Figure 9a) and yellow (Figure 9b) arrows schematically represent the important directions of current flow. The radial coordinates of full view are transformed as $r^* = r - R_{\text{Earth}} + 100\,\text{km}$.

considering the steady state current balance on Earth surface (S, Earth) (using Gauss's Law and assumption of constant conductivity):

$$0 = \oint_{\text{S,Earth}} \vec{J} \cdot \mathrm{d}\vec{S} = \sigma \oint_{\text{S,Earth}} \vec{E} \cdot \mathrm{d}\vec{S} = \sigma \frac{Q_{\text{Earth}}}{\varepsilon_0}. \tag{17}$$

It is an interesting consequence that if the total charge on Earth surface is zero and the total charge in the whole domain is zero (source current dipole creates zero charge in total), then the total charge in the atmosphere/ionosphere is zero. It means that the total (negative) atmospheric charge around the current source is equal with opposite sign to the total (positive) atmospheric charge residing in fair weather region. It is important to note that this result is coming from our symmetric model with no effects coming from the region outside the top ionospheric boundary. For example, the spatial variation of conductivity on the Earth surface will lead to nonzero total charge on the Earth surface. For additional analysis of electric charge on Earth and above Earth we refer the reader to *Dolezalek* [1988].

In Figure 9a the magnitude of current density spatial distribution around the source current dipole is illustrated during steady state of thunderstorm charging phase. The maximum current density is located around the source current dipole. The direction of current is verified to be in excellent agreement with previous results reported in the referred literature [e.g., *Tzur and Roble*, 1985]. The direction of upward current above the current dipole is schematically shown by black arrows in Figure 9a. The upward current vertically approaches the highly conducting top ionospheric boundary and is redirected horizontally along it as is schematically shown by the yellow arrows on full Earth view in Figure 9b. This highly conducting layer is responsible for equipotential top ionospheric boundary as discussed in section 2. The current circuit is closed in fair weather region at lower altitudes of the atmosphere where the current direction is normal to the Earth surface.

In Figure 10 the evolution of ionospheric potential due to the constant current dipole source is shown. The ionospheric potential obtained from simulation starts at $U_{\text{IE}} = 0\,\text{V}$ at $t = 0\,\text{s}$ as no charge is initially present. Then the ionospheric potential increases in time and reaches the steady state with value 62.6 V in about 300 s. This time corresponds to more than 3 times the dielectric relaxation time at altitude of lower source 4.5 km and means that the steady state ionospheric potential is approached with better accuracy than 1%. However, at this time, the charge density close to Earth surface is not yet in steady state regime (within the same accuracy) as the dielectric relaxation time is about 2 times longer on Earth surface and, therefore, longer simulation times are necessary to obtain steady state spatial distributions of charge density, seen in Figure 7.

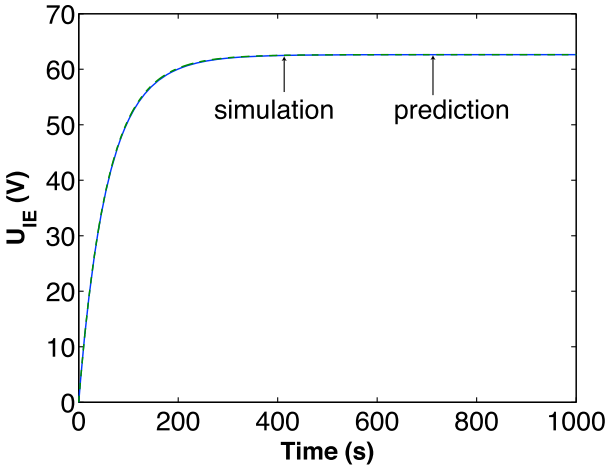

Figure 10. Ionospheric potential evolution due to constant current dipole source. Positive current 1 A is placed at 9.5 km, and negative current −1 A is placed at 4.5 km. Both currents are turned on at $t=0$. The simulation results are compared with prediction calculated from convolution of impulse responses. The relative error is less than 10^{-3}.

The predicted ionospheric potential is evaluated using equation (12) taking into account two current dipole sources:

$$U_{IE}(t) = I_s * U_{IE}^{IR}(t, h_1 = 9.5\,\text{km}) - I_s * U_{IE}^{IR}(t, h_2 = 4.5\,\text{km}), \quad (18)$$

and ionospheric potential impulse responses at the altitudes of the source currents. It is important to note that sufficient time resolution of 10^{-3} s of impulse responses is required to obtain very good agreement between simulation and prediction as seen in Figure 10. It is seen that steady state could be evaluated and therefore also interpreted as a consequence of continuous inputs of source charges and their impulse responses.

If convolution is evaluated in integral form, constant source current can be taken out of integration. Then ionospheric potential is as follows:

$$U_{IE}(t) = I_s \left[\int_0^t U_{IE}^{IR}(\tau, h_1 = 9.5\,\text{km})\,d\tau - \int_0^t U_{IE}^{IR}(\tau, h_2 = 4.5\,\text{km})\,d\tau \right]. \quad (19)$$

The equation (19) for $t \to \infty$ gives the formula for the steady state ionospheric potential U_{IE}. Having introduced a new notation M_{IE}^{IR} for time integral of impulse response, U_{IE} can be written as follows:

$$U_{IE} = I_s \left[M_{IE}^{IR}(h_1 = 9.5\,\text{km}) - M_{IE}^{IR}(h_2 = 4.5\,\text{km}) \right]. \quad (20)$$

In the steady state, the results for ionospheric potential can be connected to existing results of upward currents presented in the literature [*Holzer and Saxon*, 1952; *Driscoll et al.*, 1992]. The ionospheric potential divided by the global resistance of the atmosphere R_a gives fair weather current I_{FW}. In steady state, the fair weather current is equal to upward current above the sources I_{upw}. *Holzer and Saxon* [1952] presented an analytical formula for upward current I_{upw} above the storm for a current monopole I_s located at altitude h_0:

$$I_{upw} = I_s \left(1 - e^{-h_0/l}\right). \quad (21)$$

In the present work we can evaluate the same upward current from fair weather current I_{FW}, Ohm's law for fair weather region and using equation (20) for a monopole:

$$I_{upw} = I_{FW} = \frac{U_{IE}}{R_a} = \frac{I_s M_{IE}^{IR}(h_0)}{R_a}. \quad (22)$$

Using equation (16) and $h_{ref} = 0$ we can rewrite equation (22) in the following form:

$$I_{upw} = I_s e^{-h_0/l} \frac{M_{IE}^{IR}(0)}{R_a}. \quad (23)$$

It is important to note that in the work of *Holzer and Saxon* [1952] the grounded Earth is assumed and therefore it contains automatically image charges. In our work the Earth behaves as equipotential surface, but its potential is self-consistently calculated relative to zero potential at infinity. Therefore, to compare we have to introduce currents of opposite sign inside the Earth in our model. As any charge inside the Earth contributes to ionospheric potential difference as the charge on Earth surface, see equation (A3), we add source current of opposite sign on the Earth surface. Upward current is then obtained from equation (20) for $h_1 = h_0$ and $h_2 = 0$ using similar approach to that in equations (22) and (23):

$$I_{upw} = I_s \left(e^{-h_0/l} - 1\right) \frac{M_{IE}^{IR}(0)}{R_a}. \quad (24)$$

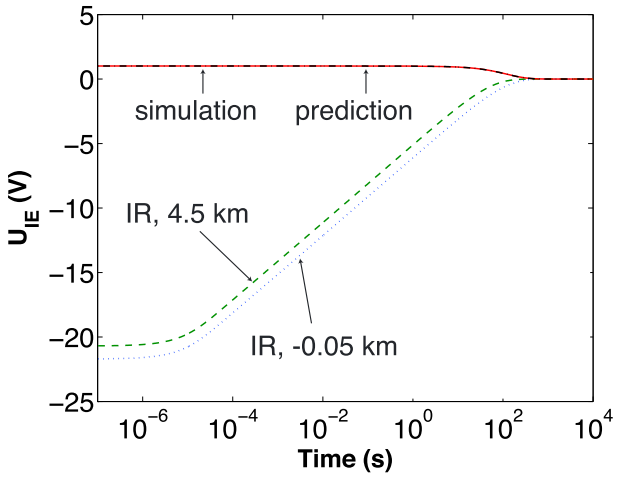

Figure 11. Ionospheric potential evolution for −CG lightning which transfers −1 C from 4.5 km to the Earth. Impulse responses for −0.05 km and 4.5 km are shown. The predicted ionospheric potential is the linear combination of impulse responses and agrees very well with simulation results.

From equations (21) and (24) it is seen that the time integral $M_{IE}^{IR}(0)$ of ionospheric potential impulse response to instantaneous input of charge at altitude 0 km is equal to negative of the global electric resistance of the atmosphere R_a. This equality is verified numerically as the global resistance of the atmosphere is $R_a = 234.9\,\Omega$ and from equation (16) we get $M_{IE}^{IR}(0) = -234.2\,\Omega$. These values are also consistent with those recently published [*Baumgaertner et al.*, 2013]. Therefore, both models give consistent results.

Equation (24) for current dipole with positive current I_s at altitude h_+ and negative current $-I_s$ at altitude h_- gives an alternative form of equation for steady state ionospheric potential:

$$U_{IE} = I_s R_a \left(e^{-h_-/l} - e^{-h_+/l}\right) . \qquad (25)$$

It is important to note that the comparison with analytical formula is done for exponential profile of conductivity with scale l defined from equation (4), as for nonexponential profiles the analytical solution and the equation (25) are not generally applicable.

3.3. Negative Cloud-to-Ground Lightning

After the charging phase of thunderstorm as part of GEC, the electric field may increase over the breakdown limit in localized regions of space and lightning discharge may occur. In this section we discuss representative model results for negative cloud-to-ground (−CG) lightning and their interpretation based on impulse response of the ionospheric potential. In Figure 1c (left) −CG lightning transferring −1 C from bottom negative charge to the Earth is schematically shown. Using principles of linearity mentioned in section 2, the charge transfer of lightning can be separated from thunderstorm charging phase. Then the results of lightning are independent of any results from thunderstorm charging phase. The model of lightning is described as follows. The lightning removes the negative charge from the position of the bottom negative charge, which is equivalent to adding positive charge of the same magnitude to the same location. The lightning adds negative charge to the Earth. As shown in Figure 1c (right) the lightning is then modeled as instantaneous introduction of the charge dipole placed at $\theta = 0°$ with positive point charge $Q_s = 1$ C at altitude $h_1 = 4.5$ km and negative point charge $-Q_s = -1$ C on the Earth surface layer (Earth surface layer is a row of model cells with height 0.1 km and therefore the surface charges are located in cell centers at $h_2 = -0.05$ km).

In Figure 11 the evolution of ionospheric potential due to −CG lightning calculated from simulation and predicted from impulse responses is shown. Impulse responses for both altitudes are also plotted. The prediction of ionospheric potential is again based on equation (12):

$$U_{IE}(t) = I_l(t, h_1) * U_{IE}^{IR}(t, h_1) + I_l(t, h_2) * U_{IE}^{IR}(t, h_2) , \qquad (26)$$

where $I_l(t)$ is the lightning current. *Rycroft et al.* [2007] used a continuous current function for the description of −CG lightning which lasted 20 ms. In the present work we use instantaneous transfer of charge using Dirac delta function $I_l(t, h_1) = -I_l(t, h_2) = \delta(t)\, Q_s$ and we have verified by running simulations that the two approaches produce same results on time scales longer than lightning duration (in this case 20 ms). The equation (26) for ionospheric potential can be rewritten in the following form:

$$U_{IE}(t) = Q_s\, U_{IE}^{IR}(t, h_1) - Q_s\, U_{IE}^{IR}(t, h_2) . \qquad (27)$$

It is seen in Figure 11 that the simulation result agrees very well with the prediction as the two curves are indistinguishable and the relative difference is less than 0.1%. The ionospheric potential U_{IE} of −CG

lightning 1.01 V, calculated from both methods, does not change significantly on time scales shorter than $t = 0.1$ s. The 1.01 V corresponding to the transfer of −1 C from an altitude of 5 km to the Earth is equal to the difference between the two ionospheric potential impulse responses at an altitude of 5 km and 0 km, at time $t = 0$ s. As both impulse responses relax in the same way for time scales shorter than $t = 0.1$ s, the ionospheric potential is constant. Then the ionospheric potential starts to decrease with most of the drop happening in the time range from 10 to 500 s. The characteristic time of ionospheric potential relaxation of −CG lightning is determined from impulse response corresponding to the charge at lower altitude (see Figure 11), which is 0 km, and therefore corresponds to the dielectric relaxation time on Earth's surface ∼177 s. For $t > 10^3$ s the ionospheric potential drops to zero. The corresponding charge distribution is zero everywhere. As we have demonstrated that convergent state of impulse response to the source point charge 1 C is the homogeneously distributed surface charge on the top ionospheric boundary, then if dipole charge configuration is input in the system, the total charge on the top ionospheric boundary at the end is zero.

Rycroft et al. [2007] and *Rycroft and Odzimek* [2010] presented results on the change of ionospheric potential due to a −CG lightning discharge. They considered the typical return stroke of 30 kA with characteristic time 0.07 ms and the amplitude of the continuing current (of 20 ms duration) 0.2 kA. Total charge transferred to the ground was −7 C. The ionospheric potential changed and reached the maximum of 3.8 kV in ∼20s. Then the ionospheric potential change relaxed to zero. The ionospheric potential change was found to be proportional to the charge moment change of lightning.

In our work the peak value of the ionospheric potential change is also found to be proportional to the charge moment change of the modeled lightning, as is shown in Appendix A. The proportionality is not exact, and a small correction in the denominator of equation (A5) is required to be analytically correct. The coefficient of proportionality 0.22 V/C/km is about 2 times higher in our results than 0.12 V/C/km in *Rycroft and Odzimek* [2010, Figure 7]. In the present work the peak value corresponds to the free space solution at $t = 0$ s, while in *Rycroft et al.* [2007] the peak value is reached in ∼20s. The relaxation after the lightning discharge in the present work is mostly determined by the dielectric relaxation time on Earth's surface 177 s. In *Rycroft et al.* [2007], characteristic time of fair weather RC circuit 165 s is enforced by adjusting atmospheric capacitance, but the time scale agrees well with results from the present more general calculations.

For a representative model evaluation of global contribution of −CG lightning discharges to the GEC ionospheric potential we use data from *Rycroft et al.* [2007]: typical −CG lightning transfers $Q_{-CG} = -7$ C from altitude 5 km to the Earth with the rate of $\nu_{-CG} = 10\,\mathrm{s}^{-1}$. The periodicity of lightning appearance is 10^{-1} s, which is less than the typical time scales discussed above (∼10 s) of modification of ionospheric potential due to −CG lightning discharge. Then the ionospheric potential U_{IE} stays almost constant, and we can approximate the −CG lightning discharge current by a constant value with magnitude:

$$I_{-CG} = |Q_{-CG}\,\nu_{-CG}| = 70\,\mathrm{A}\,. \tag{28}$$

To calculate the ionospheric potential due to −CG lightning discharge, we start again from equation (12) and adjust for two current sources at altitudes 5 km and 0 km above the Earth (with the current at $h = 0$ assumed to be negative as discussed above). We look for steady state value at $t \to \infty$ and then the equation (12) takes the following form:

$$U_{IE} = I_{-CG}\int_0^\infty U_{IE}^{IR}(t, h = 5\,\mathrm{km})\,\mathrm{d}t - I_{-CG}\int_0^\infty U_{IE}^{IR}(t, h = 0\,\mathrm{km})\,\mathrm{d}t\,. \tag{29}$$

The integrals are evaluated using equation (16) and a known value −234 V/A corresponding to altitude 0 km:

$$U_{IE} = 70\,\mathrm{A}\left[\frac{-234\,\mathrm{V/A}}{\exp(5\,\mathrm{km}/6\,\mathrm{km})} - (-234\,\mathrm{V/A})\right] = 9.3\,\mathrm{kV}\,. \tag{30}$$

This value agrees with the result 10 ± 2 kV presented by *Rycroft et al.* [2007] and is approximately 4% of the Earth's ionospheric potential 250 kV.

4. Discussion

The results in this work are based on solving the system of equations (1) and (2) using new model formulation of GEC as shown in Figure 1a. In this paper representative model conditions were chosen with the intention to produce transparent and easily tractable results. Introduction of additional physical details to the model will modify the results, and we will discuss their possible influence here.

The Poisson's equation (2) is part of the model and assumes near-field approximation, which is equivalent to the assumption that the time derivative of the magnetic vector potential is much less than the gradient of the electric potential [*Jackson*, 1999, pp. 239–246] used for the derivation of equation (2). Potential at the point of observation $\vec{r}$ due to charge density ρ at position $\vec{r}\,'$ is calculated in integral form as follows:

$$\phi(\vec{r},t) = \frac{1}{4\pi\varepsilon_0}\iiint_{V'} \frac{\rho(\vec{r}\,', t-|\vec{r}-\vec{r}\,'|/c)}{|\vec{r}-\vec{r}\,'|}\mathrm{d}V', \tag{31}$$

where c corresponds to the speed of light and $\mathrm{d}V'$ is the volume element, at the position $\vec{r}\,'$, of simulation domain volume V'. To satisfy near-field approximation the term $|\vec{r}-\vec{r}\,'|/c$ has to be small in comparison with time t. For Earth dimensions, tens of thousand kilometers, the corresponding time scale is $\sim 10^{-1}$ s. That means that the dynamics of impulse response to point charge which is happening on time scales less than 10^{-1} s is not accurate (this corresponds to the behavior for altitudes above 45 km where dielectric relaxation time is $t_{\mathrm{DRT,45\ km}} = 10^{-1}$ s). For physical cases in sections 3.2 and 3.3 the time scales of interest are longer than 10^{-1} s and therefore presented results are valid.

The exponential profile of conductivity is another assumption. The conductivity in clouds is reduced by a factor of 10 and more [*Rycroft et al.*, 2007]. Then the impulse response of point charge inside the cloud would be modified as the charge relaxation inside the cloud is longer. The preliminary results show that the integrals of ionospheric potential impulse response could be modified up to 50%. Conductivity was also assumed to be constant in time, as conductivity dependent on charge or field will break the concept of linearity, and the time-dependent conductivity will also break the concept of convolution. From the physical point of view it is expected that the conductivity can be a function of charge in proximity of big thunderstorm charges but is independent in the rest and majority of the GEC domain. The upper limit of this effect can be considered analogically to the reduction of conductivity inside the cloud as mentioned above. An example of time-dependent conductivity due to external effects is γ ray burst from magnetars [e.g., *Price and Mushtak*, 2001], which ionizes a big part of the atmosphere/ionosphere and can last for several minutes. For such case the convolution is not applicable and full simulation with time-dependent input of conductivity is necessary.

We would like to discuss the effect of spherical geometry compared to cylindrical geometry and also the effect of considering Earth as a conductor with floating potential (possible only in spherical geometry), contrary to the common assumption of Earth set to zero potential. The difference of two geometries was demonstrated in section 3.2 during comparison of upward currents. Results from this work agree with error of less than 1% with results calculated in cylindrical coordinates [*Holzer and Saxon*, 1952]. This small difference is justified in [*Driscoll and Blakeslee*, 1996]. The influence of spherical geometry is found in the nonlinear form of equations (15) and (A2), but due to the small altitudes of sources and ionosphere compared to the radius of the Earth, the equations behave linearly with altitude as expected from cylindrical geometry.

The difference of floating Earth method compared to the grounded Earth was demonstrated also in section 3.2. In grounded Earth model, the potential of Earth equal to zero is forced. The charge configurations for the equipotential Earth surface can be interpreted using the image charge theory. It is important to note that this image charge in spherical geometry is not of the same magnitude as the original charge and therefore total charge in the system including image charges is not exactly zero [*Kasemir*, 1994]; however, the difference is small [*Driscoll and Blakeslee*, 1996]. Floating Earth model offers more degrees of freedom as Earth potential is not fixed to zero and having a provision to add a quantity of charge to the Earth, based on needs of model, allows to explicitly study its effect on GEC.

5. Conclusions

The principal results of this paper are as follows:

1. The time-dependent spherical model of GEC composed of continuity equation coupled with Poisson's equation is developed. The model features Earth as a conductor with finite conductivity inside the computational domain and implicit time stepping to allow analysis of charge balance and ionospheric potential on all scales.
2. The concept of impulse response of GEC is introduced that allows effective representation of complex time dynamics of various physical quantities in the circuit using model results obtained for instantaneous deposition of a point charge. The more complex problems are then reconstructed using convolution and linearity principles.
3. For a point charge instantaneously deposited at typical thundercloud altitude, the impulse response of the charge density shows induction of the same value and polarity charge at the ionospheric boundary, while charge of the same value but opposite sign is moving down logarithmically with time and neutralizes the source point charge on time scale corresponding to the dielectric relaxation time at altitude of source point charge. The ionospheric potential is modified immediately with input of source point charge based on free space solution of Poisson's equation. Then the ionospheric potential relaxes. The high surface charge on Earth is induced under the source after the input of the source charge while weaker, and opposite sign surface charge is observed in the rest and most of the Earth. For latitude- and longitude-independent conductivity model, the total charge on the Earth is exactly zero at all times (unless the source charge is placed inside Earth).
4. For input of constant source current dipole to the model resembling the formation of two main charge centers of a thunderstorm, the convolution of source current and ionospheric potential impulse response gives evolution of ionospheric potential. The steady state ionospheric potential is then determined from the difference of time integrals of the ionospheric potential impulse responses corresponding to the altitudes of current dipole. The steady state ionospheric potential is compared using Ohm's law with steady state upward current results from existing literature and very good agreement is obtained.
5. The negative cloud-to-ground (−CG) lightning influence on ionospheric potential is studied. The −CG lightning ionospheric potential change has a peak value proportional to charge moment change of the lightning. Ionospheric potential for −CG lightning originating at altitude 5 km does not change significantly on time scales shorter than $t = 0.1$ s. Then the ionospheric potential starts to decrease with most of the drop happening in the time range from 10 to 500 s. For $t > 10^3$ s the ionospheric potential drops to zero. The results in this work confirm that global contribution of −CG lightning to the GEC ionospheric potential is about 4%, which agrees very well with results reported in [*Rycroft et al.*, 2007].

Appendix A: Ionospheric Potential Calculation

In this section the analytical calculation of ionospheric potential from a point charge $Q_c = 1$ C is presented. It describes free space solution in multisphere system as shown in Figure 1a (without any effects of conductivity). Ionospheric potential U_{IE} is defined as a difference between average potential on top ionospheric boundary and average potential on Earth, see equation (3). It is important to note that in spherical coordinates the ionospheric potential is only a function of altitude of point charge. The move in coordinates θ and φ of point charge moves correspondingly the distribution of potential, but the average value remains same. Then we can spread the point charge at $R_c = R_{Earth} + h_c$ on a spherical surface of radius $R_c = R_{Earth} + h_c$ without any change in the average ionospheric potential. Homogeneously distributed charge on the sphere produces spherically symmetric solution of potential:

$$U(r) = \frac{1}{4\pi\varepsilon_0}\frac{Q_c}{R_c}, \quad \text{for } r \le R_c,$$
$$U(r) = \frac{1}{4\pi\varepsilon_0}\frac{Q_c}{r}, \quad \text{for } r > R_c. \tag{A1}$$

Then the potential difference in between top ionospheric boundary at altitude h_{iono} and Earth due to charge Q_c at altitude $h_c > 0$ is evaluated:

$$U_{IE}(Q_c, h_c) = \frac{1}{4\pi\varepsilon_0}\left(\frac{Q_c}{R_{Earth} + h_{iono}} - \frac{Q_c}{R_{Earth} + h_c}\right) \simeq \frac{1}{4\pi\varepsilon_0}\frac{Q_c(h_c - h_{iono})}{R_{Earth}^2}, \tag{A2}$$

which for $h_{iono}, h_c \ll R_{Earth}$ is a linear function of h_c. This also can be seen in the modified equation (15) with neglected h and h_{iono} in the denominator. It is interesting to note that charge on the top ionospheric boundary $h_c = h_{iono}$ creates zero ionospheric potential U_{IE}. For charge located under Earth surface at altitude $h_c \le 0$, the ionospheric potential does not depend on h_c:

$$U_{IE}(Q_c, h_c) = \frac{1}{4\pi\varepsilon_0}\left(\frac{Q_c}{R_{Earth}+h_{iono}} - \frac{Q_c}{R_{Earth}}\right). \tag{A3}$$

In reality the charge is created in couples of opposite signs and total zero charge in simulation domain is conserved. Then it is interesting to evaluate the function of ionospheric potential created by dipole with positive charge Q_c at altitude h_+ and negative charge $-Q_c$ at altitude h_-:

$$U_{IE} = \frac{1}{4\pi\varepsilon_0}\left(\frac{Q_c}{R_{Earth}+h_-} - \frac{Q_c}{R_{Earth}+h_+}\right) = \frac{1}{4\pi\varepsilon_0}\frac{Q_c(h_+-h_-)}{(R_{Earth}+h_-)(R_{Earth}+h_+)}, \tag{A4}$$

which for $h_\pm \ll R_{Earth}$ is a function proportional to the dipole moment $p = Q_c(h_+ - h_-)$. It is interesting to note that equation (A4) also represents the potential of spherical capacitor with radii $R_{Earth} + h_-$ and $R_{Earth} + h_+$ charged with Q_c. In the special case of positive charge $Q_c = 1$ C at altitude h and negative charge $-Q_c = -1$ C on Earth surface at $h_- = 0$ km, which is used for −CG lightning modeling, the ionospheric potential is equal to the following form:

$$U_{IE} = \frac{1}{4\pi\varepsilon_0}\frac{Q_c h}{R_{Earth}^2 + R_{Earth} h} \approx \frac{Q_c h}{4\pi\varepsilon_0 R_{Earth}^2}, \tag{A5}$$

which for $h \ll R_{Earth}$ is a function proportional to the dipole moment $p = Q_c h$. It is important to note that in lightning terminology, the dipole moment p is usually referred to as a charge moment change of lightning.

The derivations of ionospheric potential are analytically precise, but for practical purposes, the linear approximation of the ionospheric potential due to dipole of charges could be used:

$$U_{IE} = \frac{p}{4.516\times10^3\ \mathrm{F\,m}}. \tag{A6}$$

Acknowledgments
This research was supported by NSF under grant AGS-1135446 to Penn State University. All data are directly available after a request is made to authors J.J. or V.P.P.

Larry Kepko thanks Michael Rycroft and another reviewer for their assistance in evaluating this paper.

References

Amestoy, P. R., I. Duff, J. L'Excellent, and J. Koster (2001), A fully asynchronous multifrontal solver using distributed dynamic scheduling, *SIAM J. Matrix Anal. Appl.*, *23*(1), 15–41, doi:10.1137/S0895479899358194.

Arfken, G., and H. Weber (2012), *Mathematical Methods for Physicists, Seventh Edition: A Comprehensive Guide*, Elsevier, Waltham, Mass.

Baumgaertner, A. J. G., J. P. Thayer, R. R. Neely, and G. Lucas (2013), Toward a comprehensive global electric circuit model: Atmospheric conductivity and its variability in CESM1(WACCM) model simulations, *J. Geophys. Res. Atmos.*, *118*, 9221–9232, doi:10.1002/jgrd.50725.

Browning, G. L., I. Tzur, and R. G. Roble (1987), A Global time-dependent model of thunderstorm electricity. 1. Mathematical properties of the physical and numerical models, *J. Atmos. Sci.*, *44*(15), 2166–2177, doi:10.1175/1520-0469(1987)044<2166:AGTDMO>2.0.CO;2.

Dejnakarintra, M., and C. G. Park (1974), Lightning-induced electric fields in ionosphere, *J. Geophys. Res.*, *79*(13), 1903–1910, doi:10.1029/JA079i013p01903.

Dolezalek, H. (1972), Discussion of the fundamental problem of atmospheric electricity, *Pure Appl. Geophys.*, *100*, 8–43, doi:10.1007/BF00880224.

Dolezalek, H. (1988), Discussion on the Earths net electric charge, *Meteorol. Atmos. Phys.*, *38*(4), 240–245, doi:10.1007/BF01054576.

Driscoll, K., and R. Blakeslee (1996), Current budget of the atmospheric electric global circuit—Comment, *J. Geophys. Res.*, *101*(D12), 17,037–17,040, doi:10.1029/95JD01534.

Driscoll, K., R. Blakeslee, and M. Baginski (1992), A modeling study of the time-averaged electric currents in the vicinity of isolated thunderstorms, *J. Geophys. Res.*, *97*(D11), 11,535–11,551, doi:10.1029/92JD00857.

Greifinger, C., and P. Greifinger (1976), Transient ULF electric and magnetic fields following a lightning discharge, *J. Geophys. Res.*, *81*(13), 2237–2247, doi:10.1029/JA081i013p02237.

Hale, L. C., and M. E. Baginski (1987), Current to the ionosphere following a lightning stroke, *Nature*, *329*, 814–816, doi:10.1038/329814a0.

Hays, P., and R. Roble (1979), Quasi-static model of global atmospheric electricity, 1. Lower atmosphere, *J. Geophys. Res.*, *84*(A7), 3291–3305, doi:10.1029/JA084iA07p03291.

Holzer, R., and D. Saxon (1952), Distribution of electrical conduction currents in the vicinity of thunderstorms, *J. Geophys. Res.*, *57*, 207–216, doi:10.1029/JZ057i002p00207.

Illingworth, A. (1972), Electric-field recovery after lightning as response of conducting atmosphere to a field change, *Q. J. R. Meteorol. Soc.*, *98*(417), 604–616, doi:10.1002/qj.49709841709.

Jackson, J. D. (1999), *Classical Electrodynamics*, 3rd ed., Wiley, New York.

Kalinin, A. V., N. N. Slyunyaev, E. A. Mareev, and A. A. Zhidkov (2014), Stationary and nonstationary models of the global electric circuit: Well-posedness, analytical relations, and numerical implementation, *Izv. Atmos. Ocean. Phys.*, *50*(3), 314–322, doi:10.1134/S0001433814030074.

Kasemir, H. (1994), Current budget of the atmospheric electric global circuit, *J. Geophys. Res.*, *99*(D5), 10,701–10,708, doi:10.1029/93JD02616.

LeVeque, R. J. (2002), *Finite Volume Methods for Hyperbolic Problems*, Cambridge Univ. Press, New York.
Lyons, R. (1997), *Understanding Digital Signal Processing*, Addison Wesley Longman, Inc., Reading, Mass.
Makino, M., and T. Ogawa (1984), Responses of atmospheric electric-field and air Earth current to variations of conductivity profiles, *J. Atmos. Terr. Phys.*, *46*(5), 431–445, doi:10.1016/0021-9169(84)90087-4.
Mallios, S. A., and V. P. Pasko (2012), Charge transfer to the ionosphere and to the ground during thunderstorms, *J. Geophys. Res.*, *117*, A08303, doi:10.1029/2011JA017061.
Mareev, E. A., S. A. Yashunin, S. S. Davydenko, T. C. Marshall, M. Stolzenburg, and C. R. Maggio (2008), On the role of transient currents in the global electric circuit, *Geophys. Res. Lett.*, *35*, L15810, doi:10.1029/2008GL034554.
Pasko, V. P., U. S. Inan, T. F. Bell, and Y. N. Taranenko (1997), Sprites produced by quasi-electrostatic heating and ionization in the lower ionosphere, *J. Geophys. Res.*, *102*(A3), 4529–4561, doi:10.1029/96JA03528.
Price, C., and V. Mushtak (2001), The impact of the August 27, 1998, γ-ray burst on the Schumann resonances, *J. Atmos. Sol. Terr. Phys.*, *63*, 1043–1047, doi:10.1016/S1364-6826(01)00014-1.
Riousset, J. A., V. P. Pasko, P. R. Krehbiel, W. Rison, and M. A. Stanley (2010), Modeling of thundercloud screening charges: Implications for blue and gigantic jets, *J. Geophys. Res.*, *115*, A00E10, doi:10.1029/2009JA014286.
Roble, R. G., and P. B. Hays (1979), Quasi-static model of global atmospheric electricity 2. Electrical coupling between the upper and lower atmosphere, *J. Geophys. Res.*, *84*(A12), 7247–7256, doi:10.1029/JA084iA12p07247.
Rycroft, M. J., and A. Odzimek (2010), Effects of lightning and sprites on the ionospheric potential, and threshold effects on sprite initiation, obtained using an analog model of the global atmospheric electric circuit, *J. Geophys. Res.*, *115*, A00E37, doi:10.1029/2009JA014758.
Rycroft, M. J., A. Odzimek, N. F. Arnold, M. Fullekrug, A. Kulak, and T. Neubert (2007), New model simulations of the global atmospheric electric circuit driven by thunderstorms and electrified shower clouds: The roles of lightning and sprites, *J. Atmos. Sol. Terr. Phys.*, *69*(17-18), 2485–2509, doi:10.1016/j.jastp.2007.09.004.
Rycroft, M. J., K. A. Nicoll, K. L. Aplin, and R. G. Harrison (2012), Recent advances in global electric circuit coupling between the space environment and the troposphere, *J. Atmos. Sol. Terr. Phys.*, *90-91*, 198–211, doi:10.1016/j.jastp.2012.03.015.
Stansbery, E. K., A. A. Few, and P. B. Geis (1993), A global model of thunderstorm electricity, *J. Geophys. Res.*, *98*(D9), 16,591–16,603, doi:10.1029/93JD01356.
Tzur, I., and R. Roble (1985), The interaction of a dipolar thunderstorm with its global electrical environment, *J. Geophys. Res.*, *90*(D4), 5989–5999, doi:10.1029/JD090iD04p05989.
Williams, E. (1996), Current budget of the atmospheric electric global circuit—Comment, *J. Geophys. Res.*, *101*(D12), 17,029–17,031, doi:10.1029/95JD02204.
Williams, E., and E. Mareev (2014), Recent progress on the global electrical circuit, *Atmos. Res.*, *135*, 208–227, doi:10.1016/j.atmosres.2013.05.015.
Williams, E. R. (2009), The global electrical circuit: A review, *Atmos. Res.*, *91*, 140–152, doi:10.1016/j.atmosres.2008.05.018.
Wilson, C. T. R. (1921), Investigations on lightning discharges and on the electric field of thunderstorms, *Phys. Trans. Roy. Soc. London A*, *221*, 73–115.